Electronic Supplementary Information

Self-templated synthesis of Co_3O_4 hierarchical nanosheets from a metal-organic framework for efficient visible-light photocatalytic CO_2 reduction

Jia-Tong Ren, Ya-Li Zheng, Kun Yuan, Liang Zhou, Ke Wu and Ya-Wen Zhang*

Beijing National Laboratory for Molecular Sciences, State Key Laboratory of Rare Earth Materials Chemistry and Applications, PKU-HKU Joint Laboratory in Rare Earth Materials and Bioinorganic Chemistry, College of Chemistry and Molecular Engineering, Peking University, Beijing 100871, China. Fax: +86-10-62756787; Tel: +86-10-62756787; Email: ywzhang@pku.edu.cn

Experimental section

Chemicals

$Co(Ac)_2 \cdot 4H_2O$ (A.R., Alfa Aesar Chemical Co. Ltd), 1,4-naphthalenedicarboxylic acid (1,4-H_2NDC, A.R., Aladdin), isophthalic acid (H_2IPA, A.R., Aladdin), $[Ru(bpy)_3]Cl_2 \cdot 6H_2O$ (bpy = 2,2'-bipyridine, A.R., Adamas Reagent Co. Ltd.) N, N-dimethylformamide (DMF, A.R., Xilong Chemical Co. Ltd), acetonitrile (CH_3CN, A. R., Beijing Tongguang Fine Chemicals Company), triethanolamine (TEOA, A.R., Beijing Tongguang Fine Chemicals Company), ethanol (A.R.) and deionized water (Millipore, 18.2 MΩ cm) were used as received. Commercial Co_3O_4 was purchased from Shanghai Macklin Biochemical Co. Ltd.

Synthesis of Co MOF nanosheets

Co MOF nanosheets (Co MOF NSs) with 1,4-H_2NDC as the ligand were synthesized by a DMF-based oil bath method. Briefly, 1 mmol (249.0 mg) of $Co(Ac)_2 \cdot 4H_2O$ and 1 mmol (216.2 mg) of 1,4-H_2NDC were mixed in 40 mL of DMF using a flask. The mixture turned into a purple suspension under stirring. After continuous stirring for 30 min, the flask was put into an oil bath (120 °C) and heated for 2 h. After the resulting mixture was cooled to room temperature, the precipitate with a pinkish purple color was collected by centrifugation, washed with DMF and ethanol several times, and finally dried in vacuum at 50 °C.

Synthesis of Co_3O_4 hierarchical nanosheets

Co_3O_4 hierarchical nanosheets (Co_3O_4 HNSs) were obtained by calcining the aforementioned Co MOF nanosheets in air at 400 °C for 2 h with a heating rate of 2 °C min^{-1}.

Synthesis of Co MOF nanoballs and Co_3O_4 nanoparticles

Co MOF nanoballs (Co MOF NBs) were synthesized by the same procedure as Co MOF nanosheets except that 1 mmol (166.2 mg) of H_2IPA rather than 1,4-H_2NDC were used in the synthesis. Co_3O_4 nanoparticles (Co_3O_4 NPs) were obtained by calcining the bluish purple Co MOF nanoballs in air at 400 °C for 2 h with a heating rate of 2 °C min^{-1}.

Characterization

Scanning electron microscopy (SEM) was carried out using a FE-SEM (Hitachi S-4800, Japan). Transmission electron microscopy (TEM), high-resolution transmission electron microscopy (HRTEM), high-angle annular dark-field scanning transmission electron microscopy (HAADF-STEM) and energy-dispersive X-ray spectroscopy (EDS) were carried out using FEG-TEM (JEM-2100F, JEOL, Japan) operated at 200 kV. X-ray diffraction (XRD) patterns were obtained on a D2-PHASER diffractometer (Bruker, Germany) using Cu-Kα radiation. Fourier transform infrared spectroscopy (FT-IR) was conducted on a Tensor-27 infrared spectrometer (Bruker, Germany) using KBr pellets. ^{1}H-NMR tests were finished on a ARX-400 NMR Spectrometer (400 MHz, Bruker, Germany). Thermogravimetric analysis (TGA) was performed under atmospheric environment using a Q600 SDT TGA system (TA, USA). Ultraviolet photoelectron spectroscopy (UPS), X-ray photoelectron spectroscopy (XPS) and valence band X-ray photoelectron spectroscopy (VB-XPS) analyses were performed on an AXIS Supra XPS spectrometer (Kratos, U.K.). The C 1s line at 284.8 eV was used to calibrate the binding energies. Nitrogen adsorption–desorption isotherm experiments were performed at 77 K on an Accelerated Surface Area & Porosimetry system (ASAP 2010, Micromeritics, USA) to determine the Brunauer–Emmett–Teller (BET) surface area and pore size distribution. CO_2 adsorption experiments were conducted on Autosorb-iQ automated gas sorption analyzer (Quantachrome, USA) at 303 K. UV-Vis-NIR diffuse reflectance spectra (UV-Vis-NIR DRS) were acquired using a UV-3600 Plus UV-Vis-NIR spectrometer (Shimadzu, Japan) equipped with an integrating sphere and $BaSO_4$ was used as a reference. Photoluminescence (PL) spectra were obtained using a FLS980 steady-state and time-resolved fluorescence spectrometer (Edinburgh Instruments, U.K.) at room temperature. Time-resolved PL decay spectra were recorded at 615 nm under the excitation of a 450 nm laser source. For steady-state PL spectra, the excitation wavelength was 450 nm from a Xe lamp. Electrochemical impedance spectroscopy (EIS) measurements were performed in a standard three-electrode system. A Pt plate and a KCl-saturated Ag/AgCl electrode were used as the counter and the reference electrode, respectively. The working electrode was a glassy carbon electrode (diameter of 5 mm) prepared by dropping 20 μL of sample-ethanol suspension (2.5 mg mL^{-1}) and 5 μL of Nafion solution (0.5

wt%) followed by fast drying. Electron paramagnetic resonance (EPR) analysis was carried out on a Bruker Elexsys E580 X-band EPR spectrometer (Bruker, Germany) at room temperature.

Photocatalytic CO_2 reduction

A quartz photoreactor attached to a closed photocatalytic system equipped with an online gas chromatograph (GC-7806) was used to evaluate the activity of photocatalytic CO_2 reduction. 20 mg of $[Ru(bpy)_3]Cl_2 \cdot 6H_2O$ and 20 mg of the catalyst were suspended in a mixture of CH_3CN, H_2O and TEOA (3:1:1 in volume, 60 mL in total) under stirring. The temperature of the reactor was kept at 288 K by circulating cooling water. Before light irradiation, the system was evacuated and filled with high-purity CO_2 (99.999 %) three times to remove the air inside thoroughly. CO_2 was then continuously bubbled into the test liquid for 1 h with a flow velocity of 100 mL min^{-1}, which was aimed to ulteriorly ensure the complete removal of air and to facilitate the sufficient dissolution of CO_2. Finally, the reactor was illuminated by a 300 W Xe lamp (Microsolar 300, PerfectLight) equipped with a UV cut-off filter ($\lambda > 400$ nm). The distance between the light source and the liquid level was approximately 11 cm, and the light intensity is approximately 500 mW cm^{-2}. During the reaction process, the pressure inside the system was approximately 1 bar. CO and H_2 were detected by a flame ionization detector (FID) and a thermal conductivity detector (TCD), respectively. Ar was used as the carrier gas. A 7980A/5975C GC-MS (Agilent, USA) was used to analyze the products of the $^{13}CO_2$ isotope photocatalytic experiment. For the photocatalytic recycling test, the as-tested photocatalyst was collected by centrifugation and washed with CH_3CN once. After that, it was used again for the next cycle.

The apparent quantum efficiency (AQE) of Co_3O_4 hierarchical nanosheets for CO production (AQE-CO) was measured using a monochromatic irradiation light at a specific wavelength by a 300 W Xe lamp equipped with a band-pass filter. The rest of the process was identical with the normal test. AQE-CO was calculated as follows:

$$\text{AQE - CO} = \frac{\text{number of generated CO} \times 2}{\text{number of incident photons}} \times 100\ \%$$

$$= \frac{n_{CO} \times N_A \times 2}{PSt\lambda/hc} \times 100\ \%$$

Wherein, n_{CO} is the mole number of generated CO; N_A is the Avogadro's constant (6.02×10^{23} mol^{-1}); P is the power of Xe lamp at the wavelength; S is the illumination area (~ 16 cm^2); t is the photocatalytic reaction time (9000 s), λ is the wavelength; h is the Planck constant (6.626×10^{-34} J s^{-1}); c is the speed of light (3×10^8 m s^{-1}). AQE for H_2 production (AQE-H_2) was also obtained during the same process and calculated using the similar formula except that n_{CO} was substituted by n_{H2} (the mole number of generated H_2). Total AQE was the sum of AQE-CO and AQE-H_2.

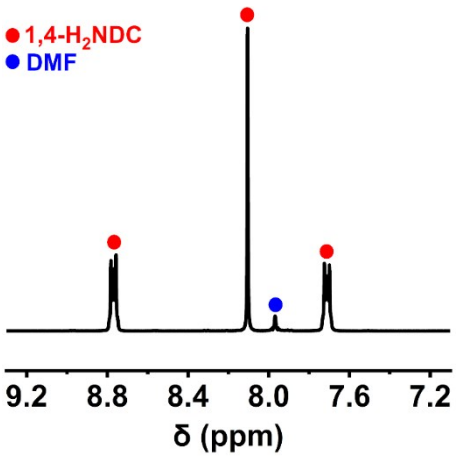

Figure S1. ^{1}H-NMR spectrum of the Co MOF formed before oil bath with 1,4-H_2NDC as the organic linker.

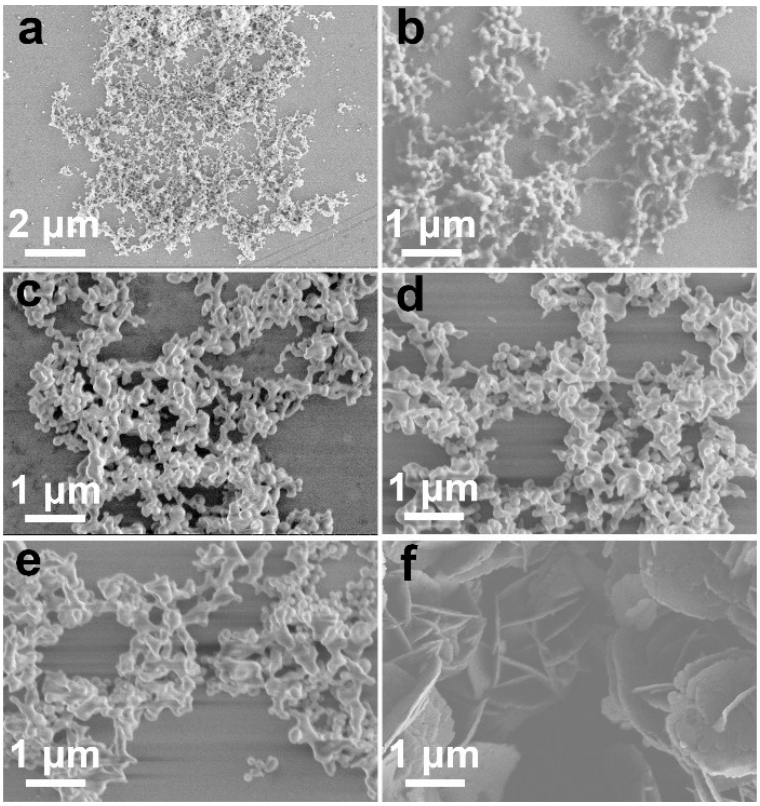

Figure S2. SEM images of Co MOF with 1,4-H_2NDC as the organic linker at (a) 0 min, (b) 10 min, (c) 20 min, (d) 30 min, (e) 60 min and (f) 120 min during the synthetic process.

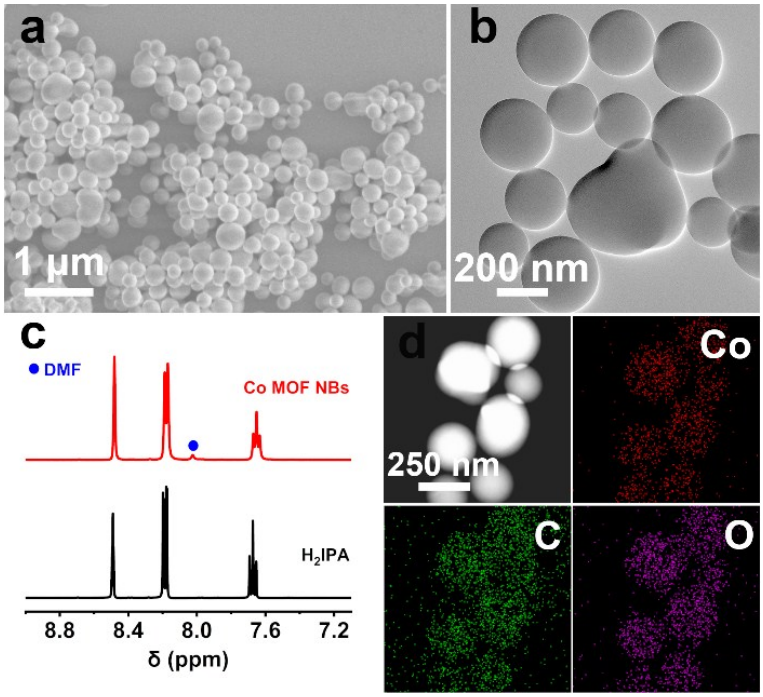

Figure S3. (a) SEM, (b) TEM and (d) EDS mapping images of Co MOF NBs with H_2IPA as the organic linker; (c) ^1H-NMR spectra of Co MOF NBs and H_2IPA.

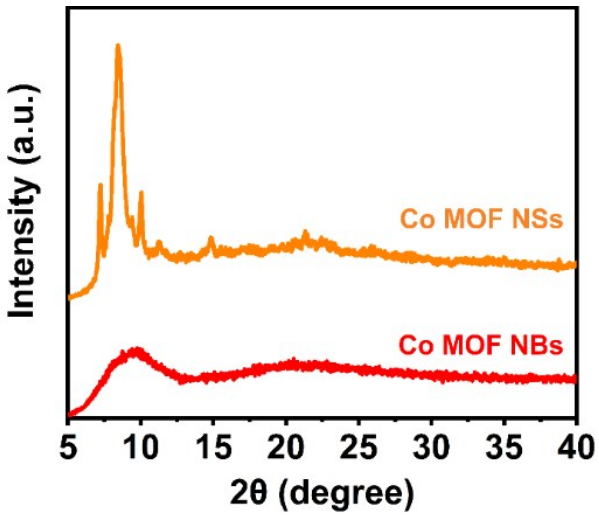

Figure S4. XRD patterns of Co MOF NSs and NBs.

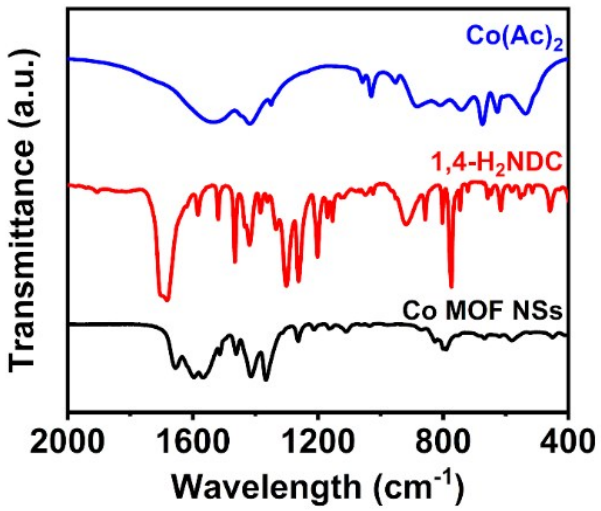

Figure S5. FT-IR spectra of Co MOF NSs as well as 1,4-H_2NDC and $Co(Ac)_2$.

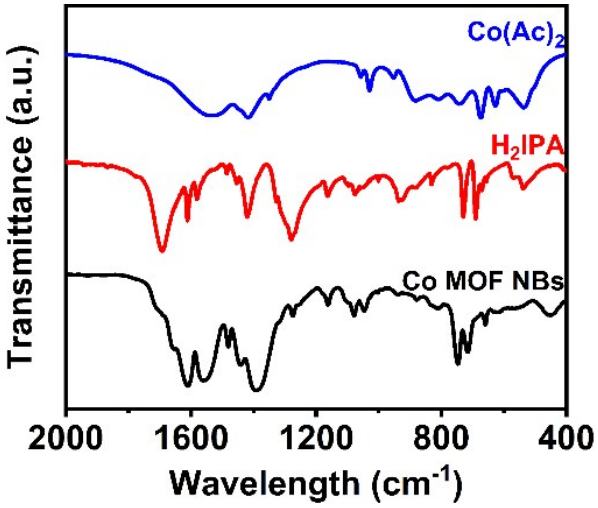

Figure S6. FT-IR spectra of Co MOF NBs as well as H_2IPA and $Co(Ac)_2$.

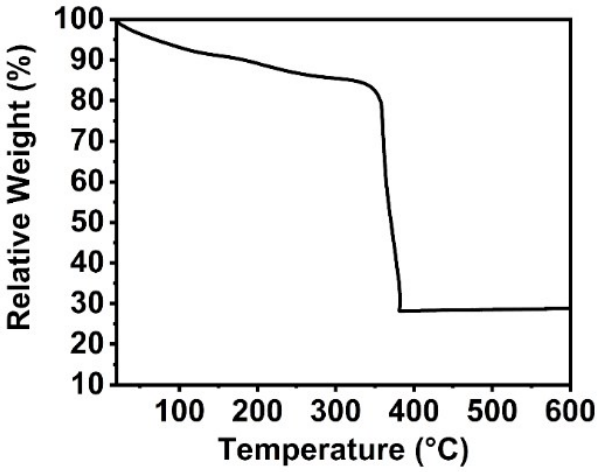

Figure S7. TG curve of Co MOF NSs in air.

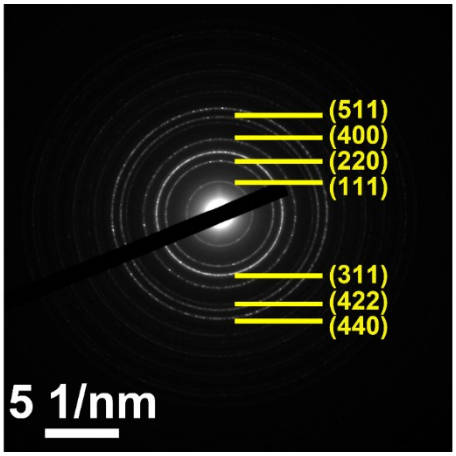

Figure S8. SAED pattern of Co_3O_4 HNSs.

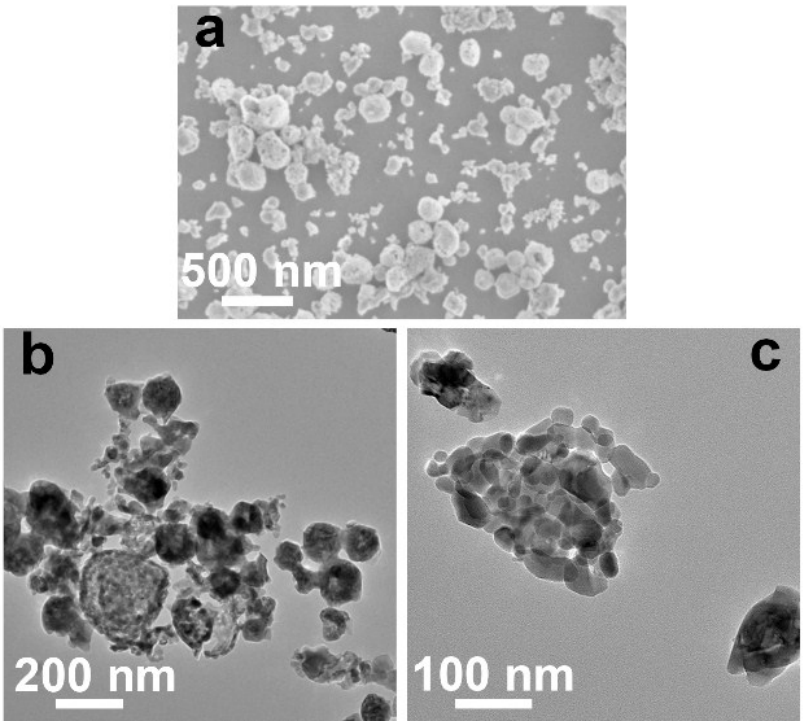

Figure S9. (a) SEM and (b, c) TEM images of Co_3O_4 NPs obtained by calcining Co MOF NBs.

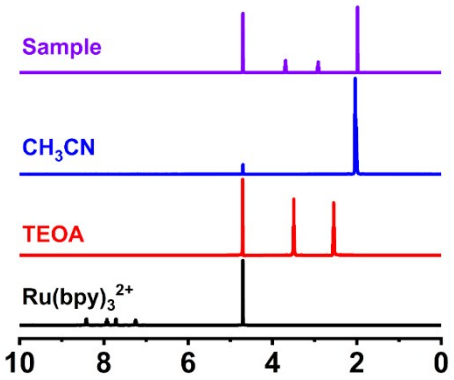

Figure S10. ^{1}H-NMR spectra of $Ru(bpy)_3^{2+}$, TEOA, CH_3CN and the sample taken from the reaction mixture after photocatalytic reaction catalyzed by Co_3O_4 HNSs.

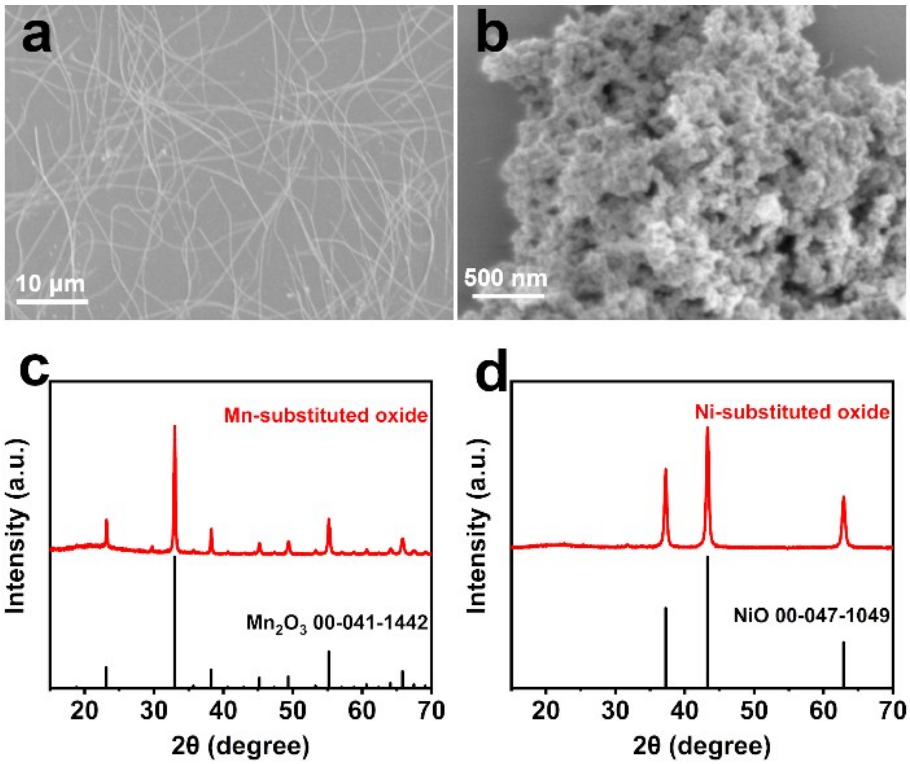

Figure S11. (a) SEM image and (c) XRD pattern of Mn-substituted calcined product; (b) SEM image and (d) XRD pattern of Ni-substituted calcined product. The synthetic process was similar with Co_3O_4 HNSs except that $Co(Ac)_2 \cdot 4H_2O$ was replaced by $Mn(Ac)_2 \cdot 4H_2O$ or $Ni(Ac)_2 \cdot 4H_2O$.

Table S1. Comparison of performance towards photocatalytic CO_2 reduction between Co_3O_4 HNSs and some newly-developed photocatalysts.

Catalyst	Light source	T (°C)	Photosensitizer /Cocatalyst	Solvent system	Products (μmol h^{-1}) /Selectivity	Ref.
Co_3O_4 HNSs	**300 W Xe lamp (λ > 400 nm)**	**15**	**$Ru(bpy)_3^{2+}$ /**	**MeCN/H_2O/TEOA 3:1:1**	**CO: 39.70 77.3 %**	**This work**
Metallic Co/C	300 W Xe lamp (λ > 420 nm)	15	$Ru(bpy)_3^{2+}$ /	MeCN/H_2O/TEOA 3:1:1	CO: 9.36 64.21 %	1
Co_3O_4 holey nanosheets	5 W LED lamp (400-1000 nm)		$Ru(bpy)_3^{2+}$ /	MeCN/H_2O/TEOA 3:2:1	CO: 4.52 70.1 %	2
Leaf-like ZIF-67	300 W Xe lamp (λ > 400 nm)	30	$Ru(bpy)_3^{2+}$ /	MeCN/H_2O/TEOA 4:1:1	CO: 3.89 ~64 %	3
Carbonized Zn/Co ZIF	100 W LED lamp (λ > 420 nm)	4	$Ru(bpy)_3^{2+}$ /	MeCN/H_2O/TEOA 5:1:1	CO: 22 ~58 %	4
NC@$NiCo_2O_4$	300 W Xe lamp (λ > 420 nm)	30	$Ru(bpy)_3^{2+}$ /	MeCN/H_2O/TEOA 3:2:1	CO: 26.2 88.6 %	5
$LaCoO_3$	300 W Xe lamp (λ > 420 nm)	30	$Ru(bpy)_3^{2+}$ /	MeCN/H_2O/TEOA 3:2:1	CO: 44.2 78.0 %	6
Hollow multi-shelled Co_3O_4 dodecahedron	200 W Xe lamp (AM 1.5G)		/ /	H_2O	CO: 0.232	7
Ni-doped $ZnCo_2O_4$	300 W Xe lamp (AM 1.5G)	25	/ /	H_2O	CO: 0.628 CH_4: 0.404	8
$CsPbBr_3$ QDs/g-C_3N_4	300 W Xe lamp (λ > 420 nm)	20	/ /	MeCN/H_2O	CO: 1.19 ~100 %	9
$ZnIn_2S_4$-In_2O_3 nanotubes	300 W Xe lamp (λ > 400 nm)	30	/ $Co(bpy)_3^{2+}$	MeCN/H_2O/TEOA 3:2:1	CO: 12.3 ~81 %	10
Au@CdS hollow particles	300 W Xe lamp (λ > 400 nm)	30	/ $Co(bpy)_3^{2+}$	MeCN/H_2O/TEOA 3:2:1	CO: 15.03 70.3 %	11

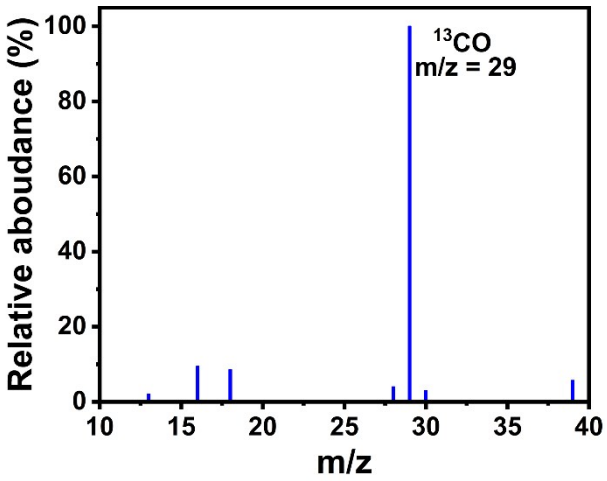

Figure S12. Mass spectrum of GC-MS analysis for the produced CO from the $^{13}CO_2$ isotope photocatalytic experiment using Co_3O_4 HNSs as the catalyst.

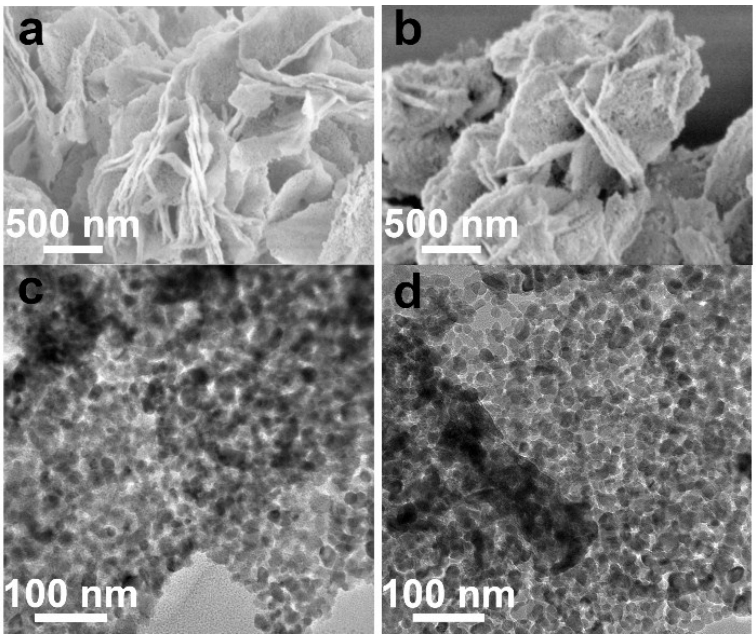

Figure S13. Electron microscope images of Co_3O_4 HNSs (a, c) before and (b, d) after the photocatalytic cyclic test.

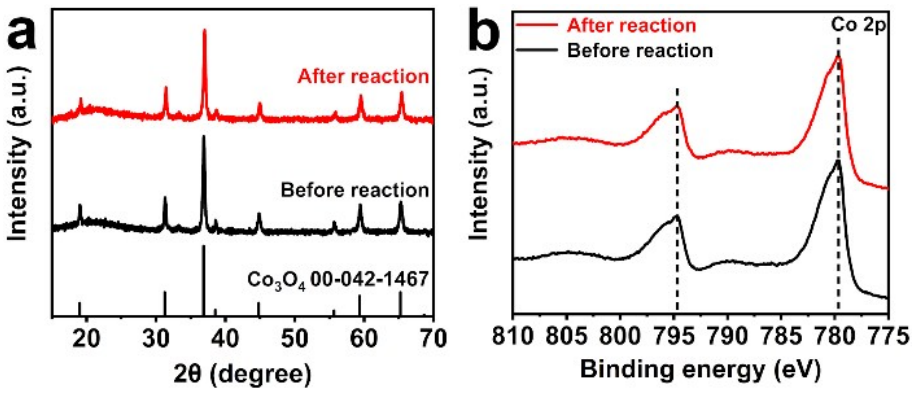

Figure S14. (a) XRD patterns and (b) Co 2p XPS spectra of Co_3O_4 HNSs before and after the photocatalytic cyclic test.

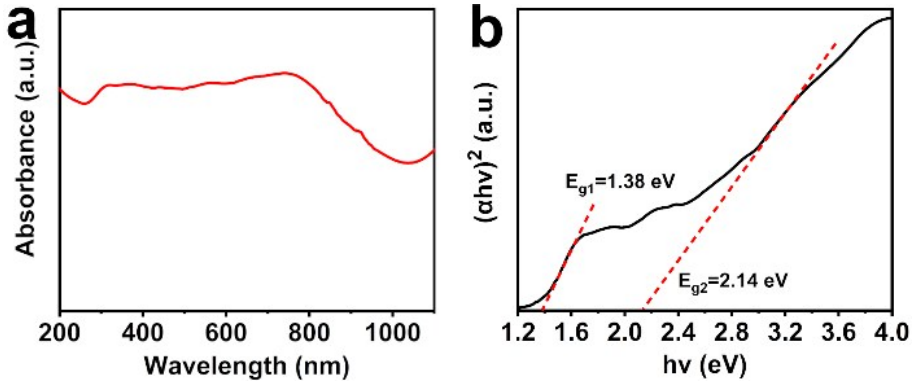

Figure S15. (a) UV-Vis-NIR diffuse reflectance spectrum and (b) Tauc plot of Co_3O_4 HNSs.

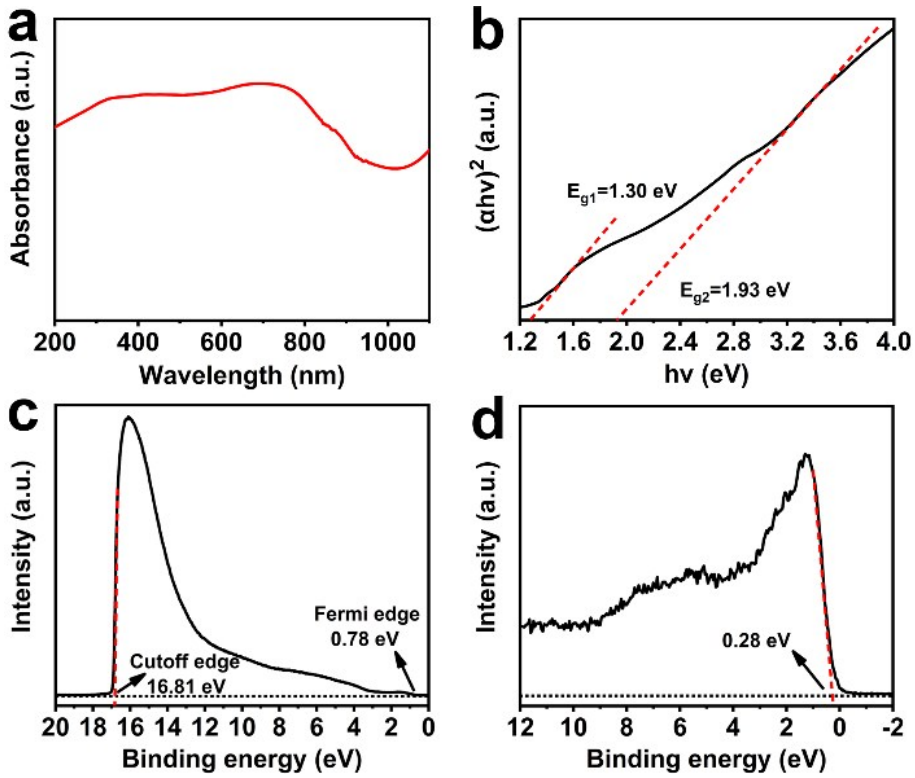

Figure S16. (a) UV-Vis-NIR diffuse reflectance spectrum, (b) Tauc plot, (c) UPS spectrum and (d) VB-XPS spectrum of Co_3O_4 NPs.

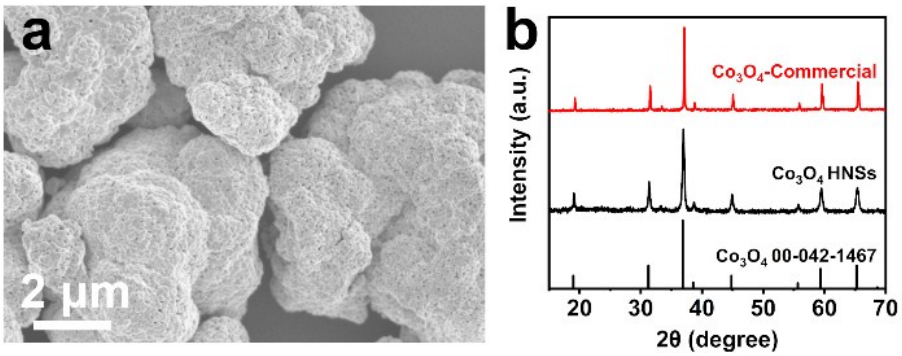

Figure S17. (a) SEM image and (b) XRD pattern of commercial Co_3O_4.

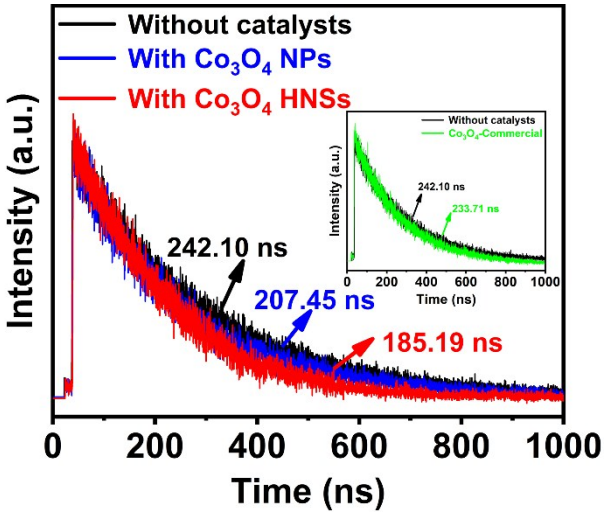

Figure S18. Time-resolved PL decay spectra of the solvent system without or with different Co_3O_4 photocatalysts. Inset is the comparison of PL lifetime between the solvent system without catalysts and with commercial Co_3O_4.

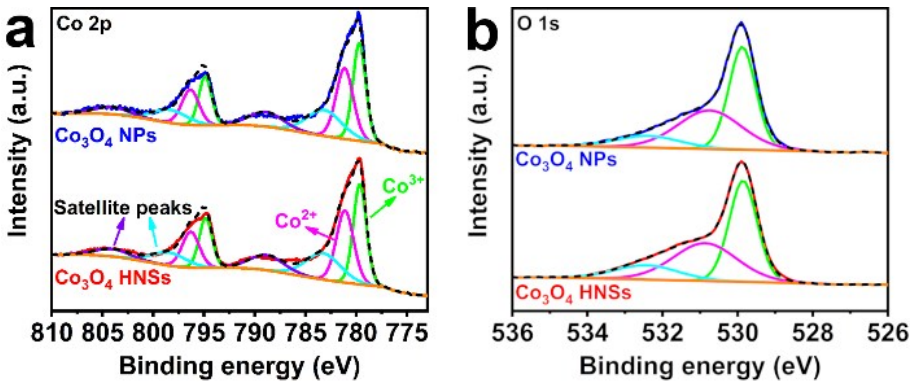

Figure S19. (a) Co 2p and (b) O 1s XPS spectra of Co_3O_4 HNSs and Co_3O_4 NPs.

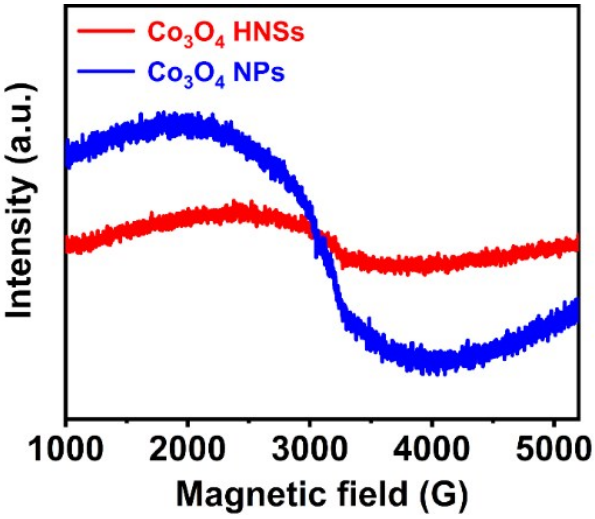

Figure S20. Room-temperature EPR spectra of Co_3O_4 HNSs and Co_3O_4 NPs.

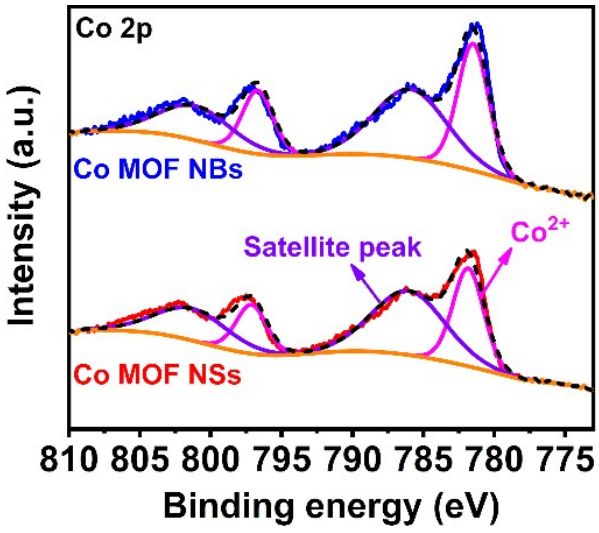

Figure S21. Co 2p XPS spectra of Co MOF NSs and Co MOF NBs.

Supplementary references

1 K. Zhao, S. L. Zhao, C. Gao, J. Qi, H. J. Yin, D. Wei, M. F. Mideksa, X. L. Wang, Y. Gao, Z. Y. Tang and R. B. Yu, *Small,* 2018, **14**, 1800762.

2 W. Y. Chen, B. Han, C. Tian X. M. Liu, S. J. Liang H. Deng and Z. Lin, *Appl. Catal. B: Environ.*, 2019, **244**, 996−1003.

3 M. Wang, J. X. Liu, C. M. Guo, X. S. Gao, C. H. Gong, Y. Wang, B. Liu, X. X. Li, G. G. Gurzadyan and L. C. Sun, *J. Mater. Chem. A*, 2018, **6**, 4768−4775.

4 Q. Q. Mu, W. Zhu, G. B. Yan, Y. B. Lian, Y. Z. Yao, Q. Li, Y. Y. Tian, P. Zhang, Z. Deng and Y. Peng, *J. Mater. Chem. A*, 2018, **6**, 21110−21119.

5 S. B. Wang, B. Y. Guan and X. W. Lou, *Energy Environ. Sci.*, 2018, **11**, 306−310.

6 J. N. Qin, L. H. Lin and X. C. Wang, *Chem. Commun.*, 2018, **54**, 2272−2275.

7 L. Wang, J. W. Wan, Y. S. Zhao, N. L. Yang and D. Wang, *J. Am. Chem. Soc.*, 2019, **141**, 2238−2241.

8 K. T. Liu, X. D. Li, L. Liang, J. Wu, X. C. Jiao, J. Q. Xu, Y. F. Sun and Y. Xie, *Nano Res.*, 2018, **11**, 2897–2908.

9 M. Ou, W. G. Tu, S. M. Yin, W. N. Xing, S. Y. Wu, H. J. Wang, S. P. Wan, Q. Zhong and R. Xu, *Angew. Chem. Int. Ed.*, 2018, **57**, 13570–13574.

10 S. B. Wang, B. Y. Guan and X. W. Lou, *J. Am. Chem. Soc.*, 2018, **140**, 5037–5040.

11 P. Zhang, S. B. Wang, B. Y. Guan and X. W. Lou, *Energy Environ. Sci.*, 2019, **12**, 164–168.